Arrays of 128x32 InP-based Geiger-mode avalanche photodiodes

Arrays of 128x32 InP-Based Geiger-Mode Avalanche Photodiodes

S. Verghese, K. A. McIntosh, Z. L. Liau, C. Sataline, J. D. Shelton, J. P. Donnelly, J. E. Funk, R. D. Younger, L. J. Mahoney, G. M. Smith, J. M. Mahan, D. C. Chapman, D. C. Oakley, and M. Brattain
Lincoln Laboratory, Massachusetts Institute of Technology, 244 Wood St., Lexington, MA, USA 02420-9108

ABSTRACT

Arrays of InP-based avalanche photodiodes operating at 1.06-μm wavelength in the Geiger mode have been fabricated in the 128x32 format. The arrays have been hermetically packaged with precision-aligned lenslet arrays, bump-bonded read-out integrated circuits, and thermoelectric coolers. With the array cooled to -20C and voltage biased so that optical cross-talk is small, the median photon detection efficiency is 23-25% and the median dark count rate is 2 kHz. With slightly higher voltage overbias, optical cross-talk increases but the photon detection efficiency increases to almost 30%. These values of photon detection efficiency include the optical coupling losses of the microlens array and package window.

Keywords: avalanche photodiodes, Geiger-mode, APD, single-photon counters, InP

1. INTRODUCTION

Avalanche photodiodes operating at shortwave infrared wavelengths (SWIR) in the Geiger mode (GmAPDs) can detect single photons with subnanosecond timing resolution [1]. Unlike linear-mode APDs, an InP-based GmAPD is temporarily biased several volts beyond its junction-breakdown voltage until it absorbs a signal photon. In less than 1 ns after injecting a photogenerated hole into its InP multiplier, milliamps of multiplied current discharge the cathode by more than a volt for virtually error-free detection of the photon-absorption event by a wide-bandwidth decision circuit. Therefore, GmAPDs have essentially zero readout noise and accommodate low-power, fast decision circuits. Individual GmAPDs are limited by their 1-bit dynamic range, their dark count rate and photon detection efficiency, and by the dead time needed to avoid afterpulsing. With GmAPDs in array format, an additional constraint on performance is optical cross-talk between neighboring pixels [2]. This effect is present in arrays of 100-μm pitch, but is especially important to characterize in 50-μm pitch arrays. This paper describes recent progress on fabricating 128x32-format GmAPD arrays packaged with microlenses and CMOS read-out integrated circuits.

2. 128X32 GMAPD ARRAYS

The photon-counting detectors described in this section are made by mating three semiconductor die to each other (Fig. 1c). Following the path of the photons, they are:

1. A 134x38 array of lenslets etched in GaP on a 50-μm pitch. The lenslets are produced either by gray-scale lithography [3] or by mass transport [4]. Some of the lenslets extend beyond the perimeter of the GmAPD array to improve the fabrication uniformity of the 128x32 array and to aid precision alignment and attachment. The purpose of the lenslets is to concentrate the light into the individual GmAPDs in the underlying InP die.
2. A 128x32 array of GmAPDs using a layer structure built in the InGaAsP/InP family of lattice-matched epitaxial layers. The layer structure is shown schematically in Fig. 1a and has been described previously [2]. The individual GmAPDs are smaller diameter (15-μm photoactive) than the array pitch allows. Such a low fill-factor design helps minimize both dark-count rate and cross section for optical cross talk.
3. A CMOS read-out integrated circuit (ROIC) that arms and disarms the individual GmAPDs. The ROIC also functions as a digital multiplexer that outputs the spatial and temporal data associated with photon detections made by the GmAPD array.

Advanced Photon Counting Techniques III, edited by Mark A. Itzler, Joe C. Campbell,
Proc. of SPIE Vol. 7320, 73200M · © 2009 SPIE · CCC code: 0277-786X/09/$18 · doi: 10.1117/12.821875

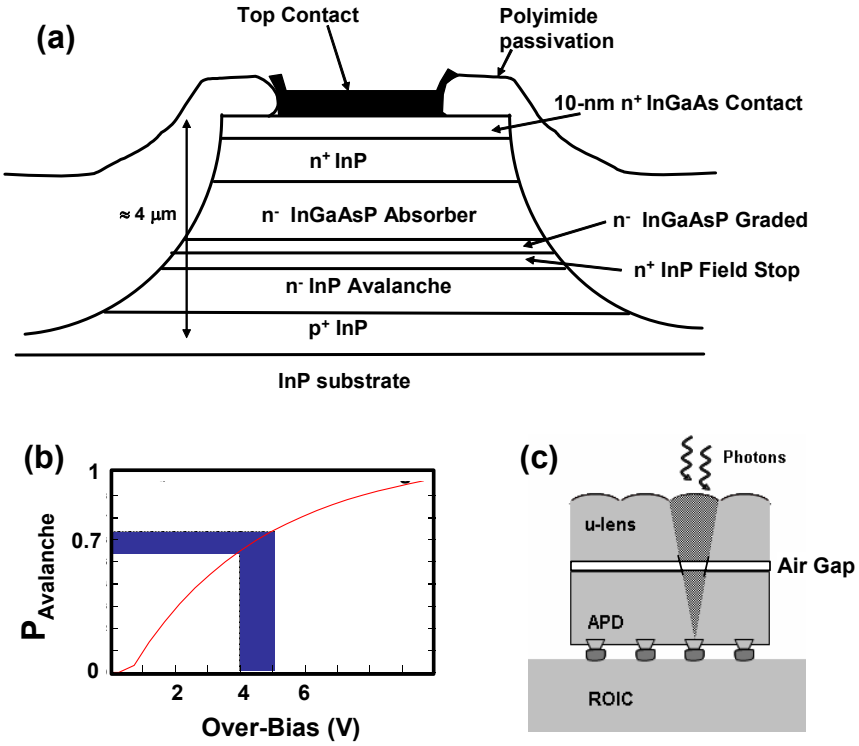

Fig. 1. (a) Cross-section of the epitaxial layers. The physical diameter of the mesa is 20 μm, but the photoactive diameter is slightly smaller (15 μm). (b) Model prediction of the probability of avalanche breakdown given that a photon has created an electron-hole pair in the absorber [5]. (c) Stack up of the three-chip assembly. The microlens and GmAPD die are both approximately 150-μm thick. There is a small air gap (6-10 μm) between the GaP lenslet array and the InP GmAPDs. All three optical surfaces are antireflection coated.

The key figures of merit for GmAPDs in large arrays are the median photon detection efficiency (PDE), median dark count rate (DCR), and the dead time needed before rearming a GmAPD that has fired to avoid after pulses. Typical values near room temperature for 128x32 arrays optimized for 1.06 μm wavelength are 26%, 10-20 kHz, and 1 μs, respectively. The DCR gets smaller with cooling (e.g. 2 kHz median at -20C), but the dead time increases (~3 μs). The dead time is only important for high frame-rate applications. The figures of merit depend on the voltage-arm bias and detector diameter as well. These effects have been described previously [2]. The emphasis of this paper is on the array's median PDE, and on how the achievable PDE is limited by the effect of optical cross-talk between individual GmAPDs.

The photon detection efficiency (PDE) is the product of three quantities:

$$PDE = \mu \cdot QE \cdot P_{AVALANCHE},$$

where μ is the optical coupling efficiency of the microlens array to the GmAPDs, QE is the probability that a photon is absorbed and creates a primary electron-hole pair, and $P_{AVALANCHE}$ is the likelihood that a primary hole is injected into the avalanche region and can initiate a large enough avalanche to trigger the ROIC's discriminator [5].

The method of estimating microlens coupling efficiency is described in Fig. 2. Even an idealized array of lenslets with perfectly curved surfaces and infinitely sharp seams between them will have coupling loss. Physical effects such as the detailed shape of the seams, deviations from a spherical lens, and surface roughness further degrade the coupling efficiency. Direct measurement of the coupling efficiency is challenging, since the focus is inside the InP substrate of the GmAPDs. Instead, a while-light interferometer (e.g. Zygo) can be used to quantify many of the as-fabricated imperfections for a few representative lenslets in an array. Those data can then be used to predict the focal length as well as the energy that will be encircled by a GmAPD of a given diameter. Fig. 2a shows a numerical prediction (including diffraction) for the intensity on a $\log_{10}$ scale at the plane of the InGaAsP absorber of a given GmAPD. A GmAPD placed at the center will encircle most of the energy that would otherwise be lost due to the low fill

factor of the detector array. Fig. 2b shows the energy that would be encircled by the GmAPD as a function of photoactive radius. The photoactive radius is typically 2.5 μm less than the physical radius of our mesa-etched GmAPDs. The annotation indicating ~81% coupling for 20-μm diameter mesas takes this into account. By using an active-alignment technique, assembly tolerances need only reduce the final coupling to between 75-80% across the array [6]. A greater source of variation across the array comes from as-fabricated lenslet-to-lenslet variations.

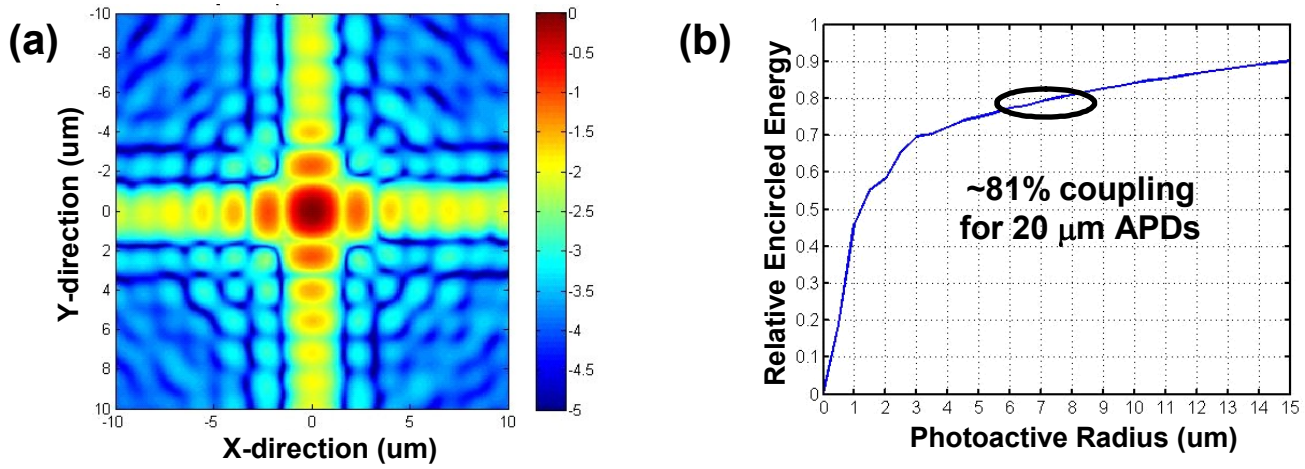

Fig. 2. (a) Numerical prediction from a diffraction code of the intensity distribution at the plane of a given GmAPD. The experimental input parameter was the Zygo-measured surface profile from a lenslet in the microlens array. The color bar is logarithmic. (b) Encircled energy as a function of photoactive radius of the GmAPD.

Assuming that a photon has been guided to the GmAPD and absorbed (typical QE is 90%), it is the probability of avalanche that determines whether it is detected. The avalanche process produces a large enough current pulse (~1-3 mA) that the odds of detecting it error free by the ROIC are near 100%. This is not the case for linear-mode APDs where the discriminator threshold must be carefully adjusted for reasonable probability of detection versus an acceptable false-alarm rate. An important constraint on the achievable PDE in GmAPD arrays, however, is optical cross-talk.

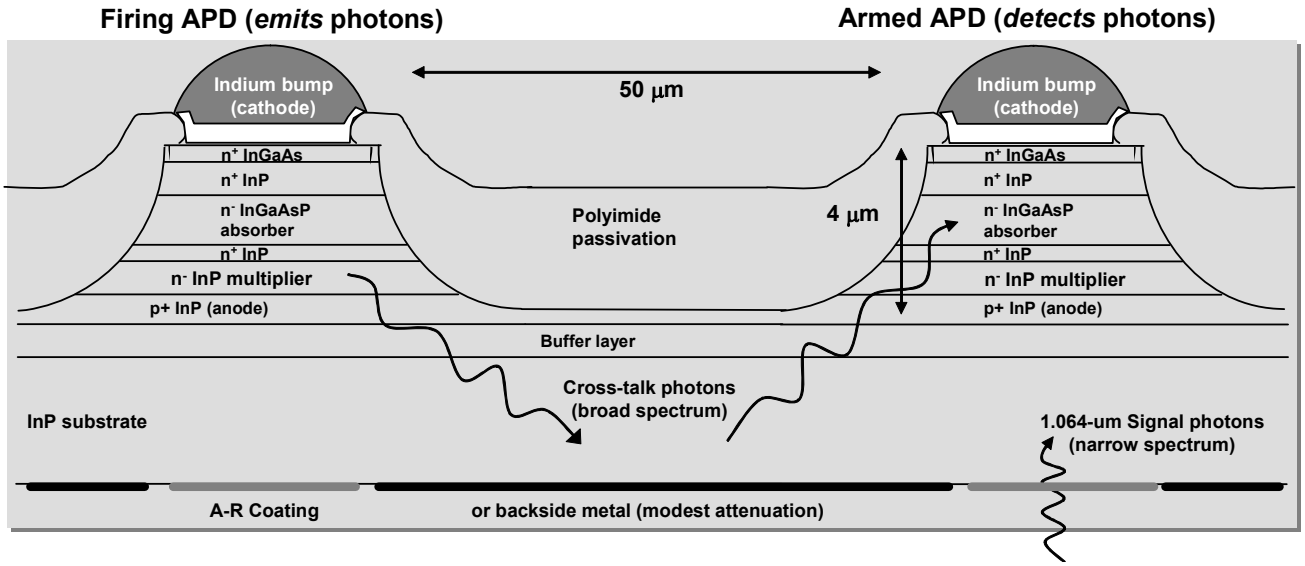

Fig. 3. Schematic of the optical cross-talk process between nearest neighbors.

Optical cross talk refers to the process where a given GmAPD goes into avalanche breakdown and thereby emits millions of photons. The majority either escape harmlessly or are absorbed by the buffer layer and substrate, but a few couple into nearby GmAPDs and cause them to avalanche. At too high overbias voltage, the process can cascade until most of the array has fired. Fig. 3 shows the process schematically for the nearest neighbor. An example of a cross-talk measurement for a 128x32 focal plane array under normal operation is shown in Fig. 4. The map was created by analyzing dark-count rate data and calculating correlations in time and space that are significantly larger than expected from the underlying Poisson-distributed dark counts. A separate paper by Younger *et al.* in these proceedings provides more detail [7].

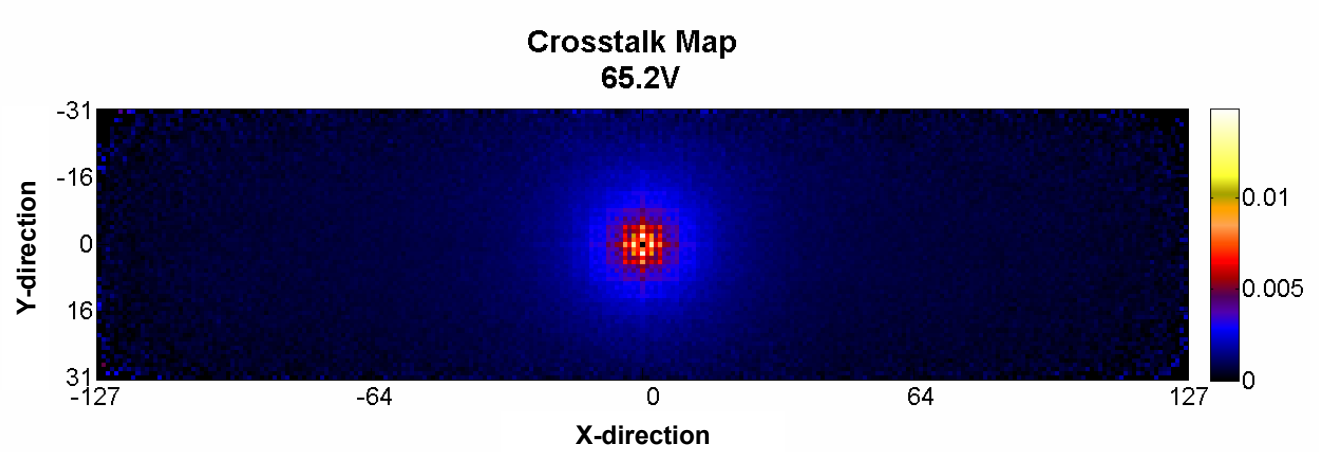

Fig. 4. Cross-talk data measured from dark-count rate statistics and averaged over all pixels in the 128x32 array. The x-y coordinates are the number of pixels away from a GmAPD that caused the primary firing. For example, a pixel in the corner of a 128x32 array can be as far as (31,127) pixels in (x,y) away from a pixel in the opposite corner. The color bar is linear, with yellow denoting ~1% chance of a nearby pixel firing due to cross talk.

Recall that Fig. 1b shows how the probability of avalanche increases with voltage overbias. Both the dark-count rate and charge flowing through a GmAPD pixel increase with overbias. For arrays of GmAPDs on 50-μm pitch, the more severe constraint is the increased charge flow which, in turn, increases the amount of light that is emitted and results in cross talk. The impact of cross talk on a GmAPD-based receiver is four-fold:

1. The point-spread function in the *x*- and *y*-directions of the observed scene broadens.
2. The temporal impulse response of the array exhibits a weak memory effect lasting up to 20 ns.
3. Pixel elements that fire due to cross talk will miss detecting subsequent signal photons.
4. Cross-talk firings in a given frame are random and contribute noise, although they obey a probability distribution function described in items 1 and 2.

The first two effects impact ladars and laser communications systems slightly differently. In either application, however, signal processing can mitigate the impact. The third effect causes a signal-dependent blockage loss, since an early photon can trigger multiple detectors and saturate that part of the array. In practice, the arrays are operated at overbias voltages low enough that no more than one cross-talk event occurs in a given 9x9 cluster of pixels centered on the primary-firing pixel. The fourth effect simply creates additional noise that is weakly correlated with the primary firing in *x*-*y* space and time. In practice, this slightly degrades the estimate of 3d location in ladar systems, or the effective SNR in a laser communications receiver.

As an example, Fig. 5 shows measurements of PDE for a recent 128x32 detector after final assembly (including microlenses and the package window). The overbias voltage was pulsed approximately 6V above the negative bias voltage, which was set slightly below breakdown and is plotted along the abscissa. Three levels of photon flux were produced from a directly modulated subnanosecond pulsed laser at 1.06-μm wavelength. The detection efficiencies plotted as solid lines are the median response of the pixels in the array. The dashed lines have been corrected for cross

talk after estimating its magnitude in the method described above. Note that just above 60V, the corrected PDE is approximately ½ of the uncorrected detection efficiency. This corresponds to one sympathetic firing due to cross talk occurring somewhere in the 128x32 array for a primary firing. At low photon flux, this is a small blockage loss. But at higher fluxes it can lead to earlier than expected saturation.

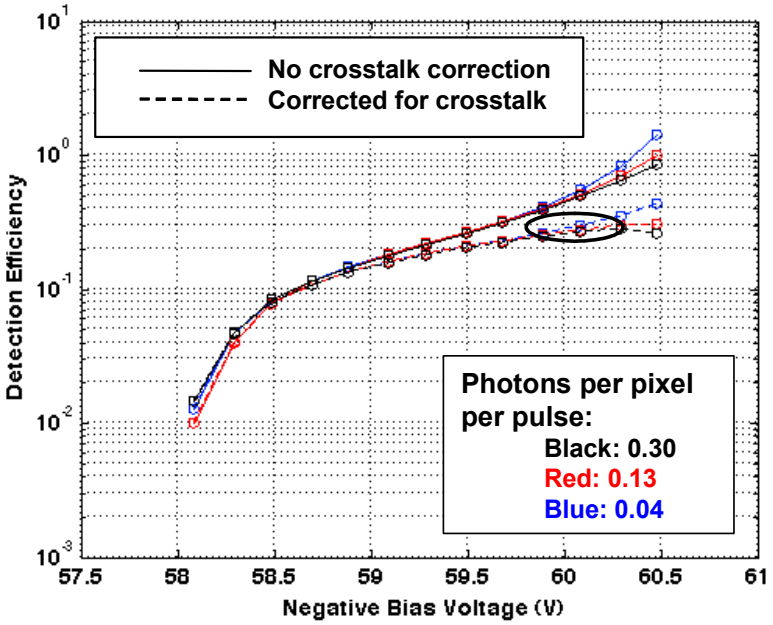

Fig. 5. Measured photon detection efficiency (PDE) for a 128x32 array (dashed lines after cross-talk correction). Three levels of optical flux at 1.06-µm wavelength were used to test the array. The median PDE of the array is between 23-30% depending on the voltage bias and, therefore, on the amount of cross talk in the array. The array temperature was -20C and the median dark count rate was approximately 2 kHz at 60.2V negative bias.

The spatial variation of the PDE is largely determined by variations in breakdown voltage uniformity across the array. This is because the current generation of ROICs supply the same anode voltage to all of the pixels in the array. Shown below in Fig. 6 is a map of the PDE for the same 128x32 array described above. The dark blue regions indicate dead pixels that did not yield through the fabrication process. The data were collected by flood illuminating the array with optical pulses from a 1.06-µm wavelength laser that was sufficiently beam expanded to provide uniform illumination.

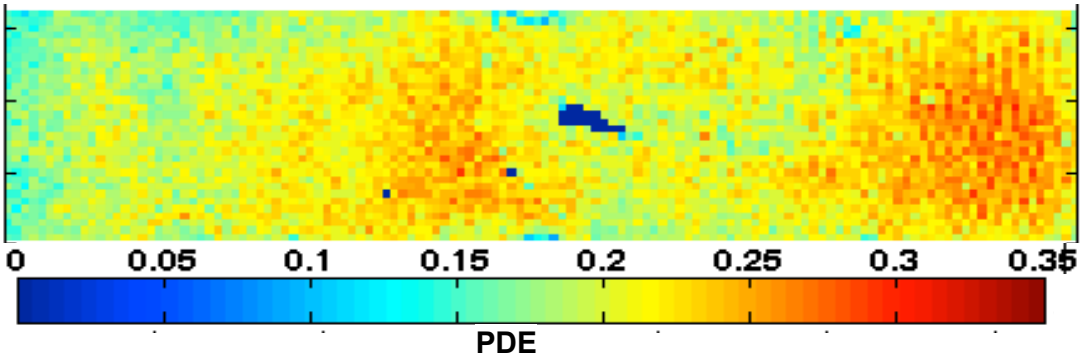

Fig. 6. Spatial map of the PDE for a fully packaged 128x32 array—including the microlenses and sapphire window.

3. OTHER ARRAY FORMATS

Other array formats are in development together with the corresponding ROICs [2]. Arrays appropriate for ladar systems tend to have rearm rates for the individual GmAPDs in the 5-20 kHz regime. This corresponds to the pulse-repetition frequency (PRF) of many of the efficient lasers available in the 1.03-1.57 μm wavelength band. The 128x32 detectors described above were optimized for 1.06-μm wavelength. The largest detectors currently under test are of the 256x64 format on 50-μm pitch. The dc power dissipated by the ROIC depends on the PRF and master clock speed. However, upper bounds on dc power are shown in Fig. 7. Power dissipated in the ROIC is the dominant heat load on the thermoelectric cooler that underlies the hybrid detector stack shown in Fig. 1c.

Arrays with a high pixel rearm rate are appropriate for laser communications systems and for ladar applications with long range gates. The underlying ROICs are sometimes referred to as asynchronous designs. Although the digital logic is synchronous, the term describes how individual GmAPDs can be armed, disarmed, and read-out independently of the other GmAPDs in the array. Asynchronous ROICs have been built and tested in the 8x8 and 32x32 format on 100-μm pitch.

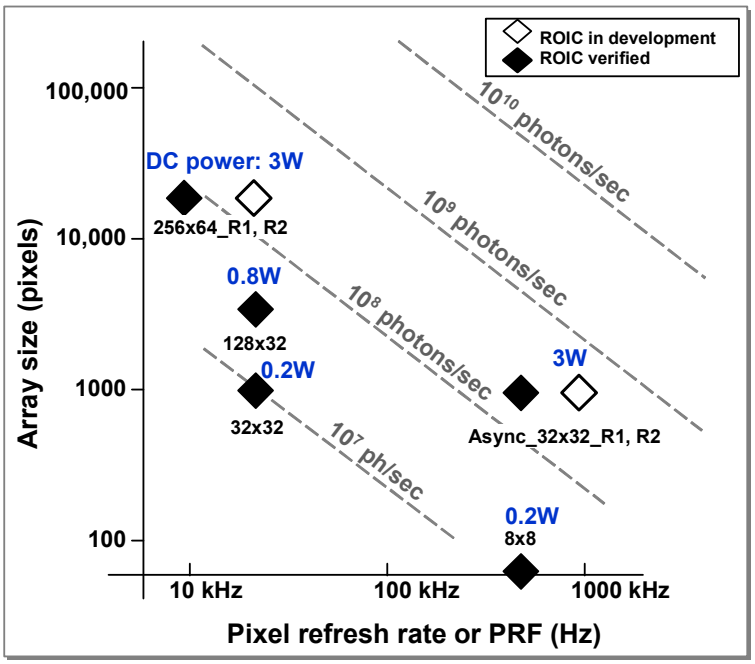

Fig. 7. Read-out integrated circuits (ROICs) for different array sizes and pulse repetition frequency (PRF). The dashed lines indicate the saturation flux of the arrays. At saturation, approximately 20% of the detectors are, on average, unavailable to detect additional incoming photons. The *R1,R2* notation refers to revisions to the ROIC.

4. FUTURE DIRECTIONS

The current GmAPD array technology is finding its way into technology demonstrators for both laser communications and ladar. Much of the interest from system designers is in the array's sensitivity and relatively small form factor. Two outstanding issues are optical cross talk and the cost to assemble the hybridized arrays.

A promising direction may be wafer fusion bonding of the InP array to the GaP microlenses. The cross talk to nearest and next-nearest neighbors should then be reduced. This is because those neighboring pixels are no longer within the critical angle for total internal reflection off of the air/InP interface due to the air gap depicted in Fig. 1c. Results from ray trace analysis of cross talk are shown in Fig. 8. The current 128x32 arrays correspond to Fig. 8a. Here, the primary firing pixel in the bottom left corner generates light which couples as depicted in Fig. 3 to nearby pixels. Fig. 8b

shows the results if the air gap is replaced by InP, as would be the case for a bonded interface. In this case, much of the light from the primary pixel escapes and the residual light bounces off of the inner surface of the GaP microlens and appears four pixels over.

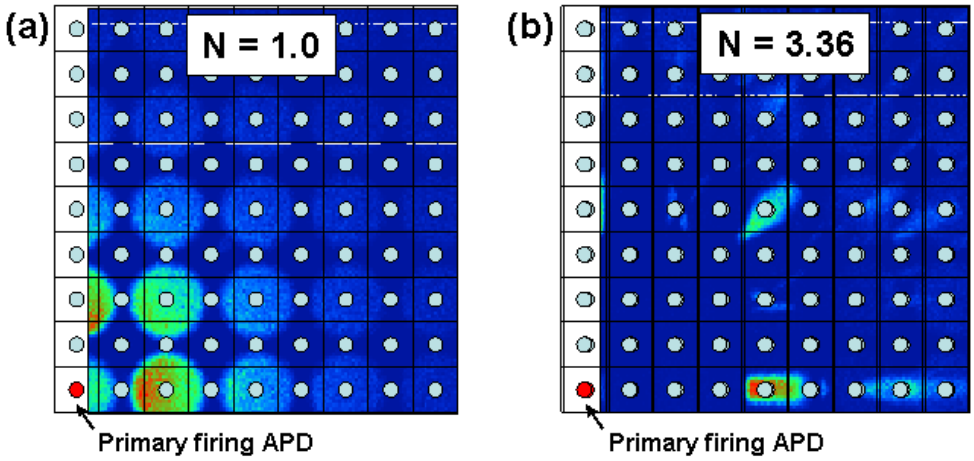

Fig. 8. Relative intensity calculations of stray light (linear color scale) resulting from a primary firing GmAPD located in the bottom left corner. (a) With an airgap between the microlens array and InP APD array. (b) With a wafer-fused interface between the GaP microlens array and InP APD array.

If wafer bonding can be demonstrated across whole wafers (2" or larger), then the wafer could be diced into hybridized die ready for bump bonding to individual ROICs. Such a process would save significant touch labor and time in epoxy-curing ovens. Fig. 9 shows a recent demonstration of an 8x8 GmAPD array that was direct bonded by thermal anneal in a phosphorous environment to a 12x12 GaP microlens array produced by mass transport. The extra microlenses accommodate alignment photodiodes outside of the 8x8 GmAPD array at the corners. With the elimination of the airgap, the reflection off the interface for normal incidence is approximately 0.06% for 1.06-μm light. At 45° angle-of-incidence, the reflection off the interface is approximately 0.3%—an angle that would cause total internal reflection in the InP for the case of the air gap.

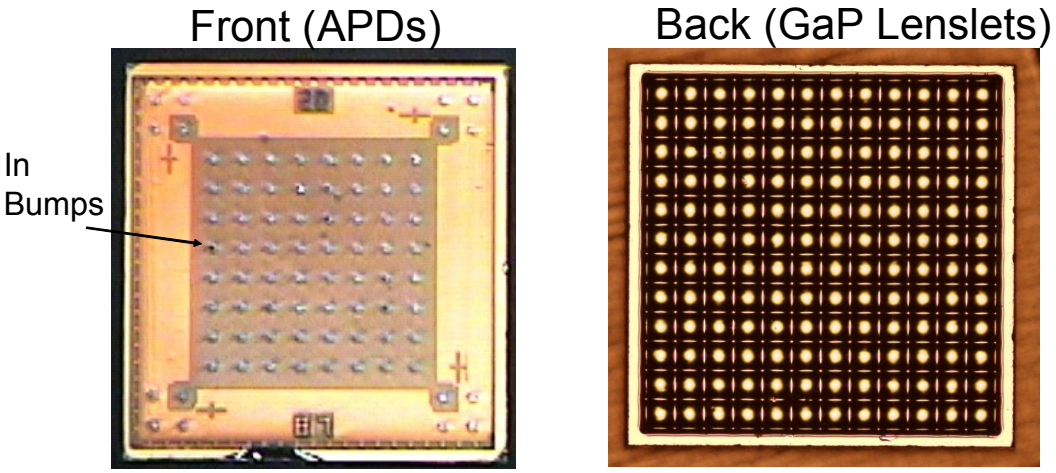

Fig. 9. First demonstration of 8x8 array of InP GmAPDs wafer bonded to an array of GaP microlenses.

The GmAPDs shown in Fig. 9 used a standard 1.06-μm design with 20-μm mesas on 100-μm pitch. The polished backside surfaces of the GmAPD and GaP-microlens wafers were first bonded by van der Waals force, and the combined wafers were heat-treated at 454C in an argon and phosphorus overpressure to form covalent bonds at the interface. The mesa-etch mask for the GmAPDs was then aligned to the microlenses on the backside by using an infrared illumination in the mask aligner. Then the finished wafer was diced into individual arrays. The assembly is pitch compatible with the 8x8 ROIC shown in Fig. 7. For test purposes, however, the wafer-bonded detector was bump-bonded to a ceramic interposer for measurement in an automated test setup. The resulting DCR was in line with DCR values measured on 8x8 arrays without direct-bonded microlenses. PDE measurements are in progress.

REFERENCES

[1] McIntosh, K. A., Donnelly, J. P., Oakley, D. C., Napoleone, A., Calawa, S. D., Mahoney, L. J., Molvar, K. M., Duerr, E. K., Groves, S. H. and Shaver, D. C., "InGaAs/InP avalanche photodiodes for photon counting at 1.06 μm," Appl. Phys. Lett. 81, 2505-2507 (2002).

[2] Verghese, S., Donnelly, J. P., Duerr, E. K., McIntosh, K. A., Chapman, D. C., Vineis, C. J., Smith, G. M., Funk, J. E., Jensen, K. E., Hopman, P. I., Shaver, D. C., Aull, B. F., Aversa, J. C., Frechette, J. P., Glettler, J. B., Liau, Z. L., Mahan, J. M., Mahoney, L. J., Molvar, K. M., O'Donnell, F. J., Oakley, D. C., Ouellette, E. J., Renzi, M. J., and Tyrrell, B. M., "Arrays of InP-based avalanche photodiodes for photon counting," IEEE J. Sel. Topics in Quantum Electron. 13, 867-883 (2007).

[3] Liau, Z. L., "Mass transport: Semiconductor microstructure fabrication by surface energy," Mater.Sci. Eng. R: Rep. R42, 41–63 (2003).

[4] MEMS Optical, Inc (www.memsoptical.com).

[5] Donnelly, J. P., Duerr, E. K., McIntosh, Dauler, E. A., Groves, S. H., Vineis, C. J., Mahoney, L. J., Molvar, K. M., Hopman, P. I., Jensen, K. E., Smith, G. M., Verghese, S. and Shaver, D. C., "Design considerations for 1.06-μm InGaAsP-InP Geiger-mode avalanche photodiodes," IEEE J. Quantum Electron. 42, 797-809 (2006).

[6] Funk, J. P., et al., {Microlens alignment paper in this issue}, Proc. SPIE, (2009).

[7] Younger, R., et al., {Cross-talk paper in this issue}, Proc. SPIE, (2009).